05

Electron lithography of non-simply patterned magnetic mesoparticles

© D.A. Tatarskiy,[1,2] E.V. Skorokhodov,[1] I.Yu. Pashen'kin,[1] S.A. Gusev[1]

[1] Institute of Physics of Microstructures, Russian Academy of Sciences,
603087 Afonino, Kstovsky District, Nizhny Novgorod Oblast, Russia
[2] Lobachevsky State University,
603022 Nizhny Novgorod, Russia
e-mail: tatarsky@ipmras.ru

Received May 4, 2024
Revised May 4, 2024
Accepted May 4, 2024

Currently, patterned magnetic structures are of great interest in connection with their potential application in spintronics as generators of microwave radiation and memory elements. In particular, two-dimensional lattices of ferromagnetic disks, in which the vortex magnetization distribution is realized, are a promising system. In this work, the latest methods of electron lithography and ion etching have been developed, allowing for a high degree allows to get high-quality particles of a given shape and size. A study of the microstructures and magnetic states of non-simply connected magnetic particles from permalloy films was carried out using analytical and Lorentz transmission electron microscopy. The experimental results demonstrate good agreement with the data obtained by micromagnetic modeling.

Keywords: electron lithography, ion etching, Lorentz transmission electron microscopy.

DOI: 10.61011/TP.2024.07.58799.147-24

Introduction

It is well known that vortex magnetization pattern occurs in ferromagnetic mesoscopic discs in some geometry range [1,2]. There are two regions in the magnetic vortex: in one region, magnetization is in the disc plane and can be whirled clockwise or counterclockwise, such region is called the vortex shell. Whereas in the central region, magnetization orientation uncertainty occurs in the plane and magnetization is oriented normally to the disc, such region is called the vortex core. The vortex shell occupies the most part of the disc volume, while the core size is maximum 10 nm. To achieve the magnetic vortex, the disc shall have certain relations between diameter and thickness. In case of low disc thickness compared with disc diameter (thin plate), quasi-uniform state in plane will occur in the disc, and in case of large thickness (nanowire) — there will be uniform state along the cylinder center line. In case of large diameter, multivortex states might also exist. As it follows from simple physical considerations, in the absence of interactions that release chiral degeneracy (e.g. the Dzyaloshinskii Moriya interaction), there is four-fold degeneracy of states that differ in shell vorticity and magnetization orientation in the core.

For patterned particles of ferromagnetic films consisting of various configurations of overlapping discs, the number of states is much higher. Double discs and disc chains are a promising object for a multivortex spin oscillator [3,4]. Two-dimensional lattices of several overlapping discs represent a multiply-connected system for magnetic memory [5]. Fabrication of such types of particles requires employment of precision electron-beam lithography to produce discs from solid films with various overlap of holes with desired shape and sizes between these discs. A special problem in this case is to obtain holes between discs in such lattices due to the proximity effect in the electron-beam lithography. It has been already demonstrated before that „vortex−vortex“ and „vortex−antivortex−vortex“ type patterns can be obtained in particles in the form of two overlapping discs [6]. Antivortex is another magnetic soliton and, therefore, it will also participate in collective behavior and induce considerable distortions into the phase synchronization of self-oscillations of neighboring vortices [4]. The next step towards achievement of two-dimensional lattices is to form particles consisting of four overlapping 2×2 discs. The problem in this case is to obtain a hole with a predefined size in the center of a particle between discs, whose configuration defines magnetic states in such elements. Thus, the aim of this study is not only to improve the electron-beam lithography process conditions to fabricate shaped magnetic elements, but also to show what kind of magnetic patterns might occur in such particles depending on their topology.

It has been shown previously that the Lorentz transmission electron microscopy is used to control [7,8] magnetic states in mesoscopic ferromagnetic particles [6,9,10]. By combining the Lorentz and analytical electron-beam microscopy methods [11], it also becomes possible to directly estimate the quality of patterned element boundaries and microstructural quality of samples that may also affect the magnetic properties of particles. Note also that the advantage of the Lorentz microscopy methods is that the orientation of magnetic vortex shell vorticity is recorded directly, unlike with magnetic-force microscopy methods

where the contrast depends on scattering fields and elliptic particles, rather than round ones, shall be made to determine shell vorticity [12].

The literature addressed the effect of the type of used electron-beam resist [13–16] and of the resist annealing modes before and after exposure on the parameters of the obtained structures [17]. The study proposes and uses two electron-beam lithography methods using polymethyl methacrylate (PMMA) as the resist [18–20]. Material structure and magnetic states of non-simply connected particles produced from permalloy films are studied by the analytical and Lorentz transmission electron microscopy methods. The key difference in the proposed lithography procedures is associated to the difference in the ion etching of exposed structures. The study demonstrates that the usage to low-energy etching makes it possible not to use additional metallization layers to improve the geometrical quality of the final structure.

1. Samples and methods

We use the AJA high-vacuum magnetron sputtering system for thin metallic films deposition.. Residual gas pressure in the evaporation chamber did not exceed $3 \cdot 10^{-7}$ Torr, the operating argon pressure during sputtering was equal to $2 \cdot 10^{-3}$ Torr. The permalloy (Ni_3Fe, Py) film, from which patterned mesoparticles were produced later, was grown from one Ni_3Fe target. Film thickness was defined from previous growth rate measurements depending on the sputtering time. The film growth rate was determined by measuring the test layer thickness using the small-angle X-ray radiation reflection method on CuK_α $\lambda = 1.54$ Å on the Discover D8 (Bruker) diffractometer and was equal to 0.1 nm/s.

The electron-beam lithography was performed using the SUPRA 50VP (Carl Zeiss) scanning-electron microscope with the ELPHY Plus (Raith) lithography attachment. Magnetic states and structure of lithographed particles were examined using the LIBRA 200MC (Carl Zeiss) transmission electron microscope adapted for the Lorentz microscopy (LTEM) operations.

As mentioned above, achievement of ferromagnetic disc lattices with vortex magnetization pattern is of major interest. In this case, to improve the electron-beam lithography methods, it is convenient to use two-dimensional lattice cell — a particle in the form of overlapping 2×2 discs with a central hole. It is well known that the vortex magnetization pattern is formed, in particular, in ferromagnetic discs made from Py film with a diameter of1 μm and thickness of 40 nm [21]. For LTEM measurements, the film was deposited onto commercial amorphous 100 nm Si_3N_4 substrates on the Si (100) base. Whereas, a window is opened on the Si side by the chemical etching method [22], where amorphous Si_3N_4 is hanging freely as a membrane and allows testing of the obtained structures by the Lorentz and analytical transmission electron microscopy methods. Magnetic patterns in the discs were examined by the Fresnel (defocusing) method that records the phase contrast associated with the non-uniform magnetization pattern. To achieve the contrast, significant defocusing is necessary and was performed by varying the excitation of the first projection electron lens in the transmission electron microscope in the low magnification mode. We used defocusing -3 mm as corresponding to the best Fresnel phase contrast recording conditions. The quality of boundaries of the obtained structures was examined using bright-field microphotographs made in the common transmission electron microscopy mode.

To form shaped nanoparticles by the electron-beam lithography method, it is a good practice to use high-resolution negative resists that simultaneously have high resistance in ionic and plasma-enhanced chemical etching processes to form shaped nanoparticles by the electron-beam lithography method. However, this type of resists is made abroad and, therefore, is unavailable now, while domestic production has not been launched yet. Therefore it was decided to use the inversion electron-beam lithography with PMMA. The first option employed a well proven procedure using auxiliary metallic films whose resistance to ionic and plasma-enhanced chemical etching was much higher that of PMMA. $Ni_3Fe(40\,nm)/V(25\,nm)/Cu(10\,nm)/Pt(5\,nm)$ structure was formed on a substrate by the magnetron sputtering method. Then the positive electron-beam resist was applied to the deposited film by the spin-coating method: 120 nm PMMA 950 polymethyl methacrylate. Intermediate metallic V/Cu/Pt mast was used due to insufficient resistance of the electron-beam resist to ionic etching. V and Cu were chosen due to considerably different etching rates of these materials: Cu is etched much faster than V in argon plasma, while V is more easily removed by freon-plasma-enhanced chemical etching. Such selectivity provides quite thick particles of V mask necessary for etching thick structure layers.

In resist layer, a pattern with desired configuration was exposed to 10 keV electron beam in resist layer. The does was $7000-9000\,mC/cm^2$ with a bean current of 0.02 nA. exposure with this does makes the PMMA 950 resist negative. The negative PMMA 950 demonstrates high contrast (higher than 10), which in turn reproduces properly the shape of structures included in the mask and to minimize the proximity effects. Unexposed electron resist was removed by means of one-minute holding in acetone. Thus, a lithographic mask was formed and then the copper and platinum layer as well as exposed resists were etched in argon. Etching was performed at an operating pressure of $2 \cdot 10^{-3}$ Torr and accelerating voltage of 1200 V. This etching mode ensures an etching rate of 10 nm/min for metallic films. Etching rate for the exposed electron-beam resist is 60 nm/min.

Plasma-enhanced chemical etching in $CF_4 + O_2$ removed the V layer in Cu mask. Partial pressures of CF_4 and O_2 for plasma-enhanced chemical etching were equal to $2.3 \cdot 10^{-3}$ and $7 \cdot 10^{-4}$ Torr, respectively, and accelerating

voltage of 800 V. After this, permalloy etching by argon ions in the obtained V mask was repeated. V etching rate was 1 nm/min, while the Py etching rate was 4 nm/min. V mask residues are removed with hydrogen peroxide.

In the second case, the same procedure was used. $Ni_3Fe(40\,nm)/Pt(5\,nm)$ structure was formed on a substrate by the magnetron sputtering method. Then the positive electron-beam resist was also applied to the substrate by the spin-coating method: 120 nm PMMA 950 polymethyl methacrylate. Then electron-beam exposure was performed by doses within $7500-9000\,mC/cm^2$ at the beam current of 0.02 nA. Development was performed in acetone during 1 min. Ionic etching in argon was performed at an operating pressure of $6 \cdot 10^{-4}$ Torr and accelerating voltage of 500 V. Before etching chamber evacuation, it was preliminary purged with extra pure nitrogen to remove atmospheric vapor and oxygen from the chamber. This etching mode ensures an etching rate of 4 nm/min for permalloy films. Etching rate for the electron-beam resist is 10 nm/min. Note that such etching rate is much lower than the electron-beam resist etching rate using the first method and avoids using additional Cu and V masks. Considerable mask thickness reduction makes it possible to improve spatial resolution of this lithography method. Therefore, the absence of intermediate metallic masks allows more accurate control of the hole shape in mesoparticles because there are no geometrical abnormalities of the etching processes in relatively narrow places between the metallic mask elements.

All produced films were studied by the analytical transmission electron microscopy. The electron microdiffraction was used to analyze the composition of the produced films. It is known that such films have polycrystalline structure, diffraction pattern is represented in this case as a set of concentric rings. The ring diameters are used to determine the distances between atomic planes in a crystal structure and identify a structural type in the film by comparison with the literature data. Moreover, the autocorrelation analysis of the polycrystalline films themselves is used to determine the mean crystallite size. In the first approximation, we will consider that nanocrystallites have axially symmetric shape, i.e. may be approximated by circle. Such approximation is justified because the substrate holder rotates during film sputtering at a rate higher than the formal growth rate of one monoatomic layer, and, therefore, film growth may be regarded as isotropic in planar orientations. In this case, to determine the mean crystallite size, the desired autocorrelation function width at half maximum shall be normalized to an additional form factor associated with the expected crystallite shape. In our case, this form factor is equal to 1.23 [23,24].

Magnetic states in patterned structures were simulated numerically in MuMax3 package on the basis of numerical integration of the Landau–Lifshitz–Gilbert equation [25]. The calculations used the following material parameters of Py: saturation magnetic moment $M_s = 800\,kA/m$, exchange constant $J = 13 \cdot 10^{-12}\,J/m$, anisotropy constant $K = 0$, attenuation parameter $\alpha = 1$. The simulation used a $512 \times 512 \times 1$ rectangular grid with mesh $4.3 \times 4.3 \times 40\,nm^3$. Thus, the mesh in the sample plane is lower than the exchange length in permalloy ≈ 5.7 nm. Simulation was performed in a zero external field. Vortex patterns in each of the discs were initially set in particles with a pre-defined shape (with and without hole), then the system energy was minimized during integration of the Landau–Lifshitz–Gilbert equation, from which precession term was excluded, by the expanded third-order Runge-Kutta method (Bogacki Shampine method) with adaptive fitting of time step. It is believed that the system has achieved local metastable minimum energy when energy variation on each step becomes lower than the computer calculation error.

Two fundamental types of micromagnetic patterns were studied. In one case, magnetic vortex shell vorticities in neighboring discs were alternated such that singularities in the form of a domain wall or antivortex were not formed between the neighboring discs. In the other case, shell vorticities coincided with one of the neighboring disc, but differed from another one. With such pattern, a singularity in the form of a domain wall or antivortex could be formed between the discs with the same shell vorticity. Such magnetization pattern has higher energy compared with the first case, but, as shown previously [10], states with antivortices are metastable and are observed in overlapped double discs, and such states should be expected in the particles addressed herein.

The obtained micromagnetic patterns was used to calculate the Fresnel contrast [26] obtained in the transmission electron microscope. The Fresnel contrast is known to be proportional to z-component of the magnetization rotor. For investigation of magnetic vortices by the Fresnel method, bright (dark) spot in the center of the vortex will indicate a vortex with the shell whirled counterclockwise (clockwise). Analysis of more complex magnetization patterns requires calculations and the Fresnel contrast no longer has such simple interpretation.

Analysis of electronic micrographs, microdiffraction rings was performed in Gatan Microscopy Suite 3.5.0 (GMS) software added with DiffTools 7.0 diffraction pattern processing module. This software was also used to simulate the Fresnel contrast using the script written in Python built in GMS environment.

2. Findings and discussion

Magnetic simulation has shown that both proposed magnetization patterns are metastable (Figure 1, *a, b*). However, there is considerable difference with and without the hole in the center of the particle. Thus, when vortex shell vorticities in neighboring discs alternate, then antivortex is formed in a particle without hole in the center. The Fresnel contrast in the form of intersecting bright and dark strips is the characteristic feature of antivortex formation in the experiment (Figure 1, *d*).

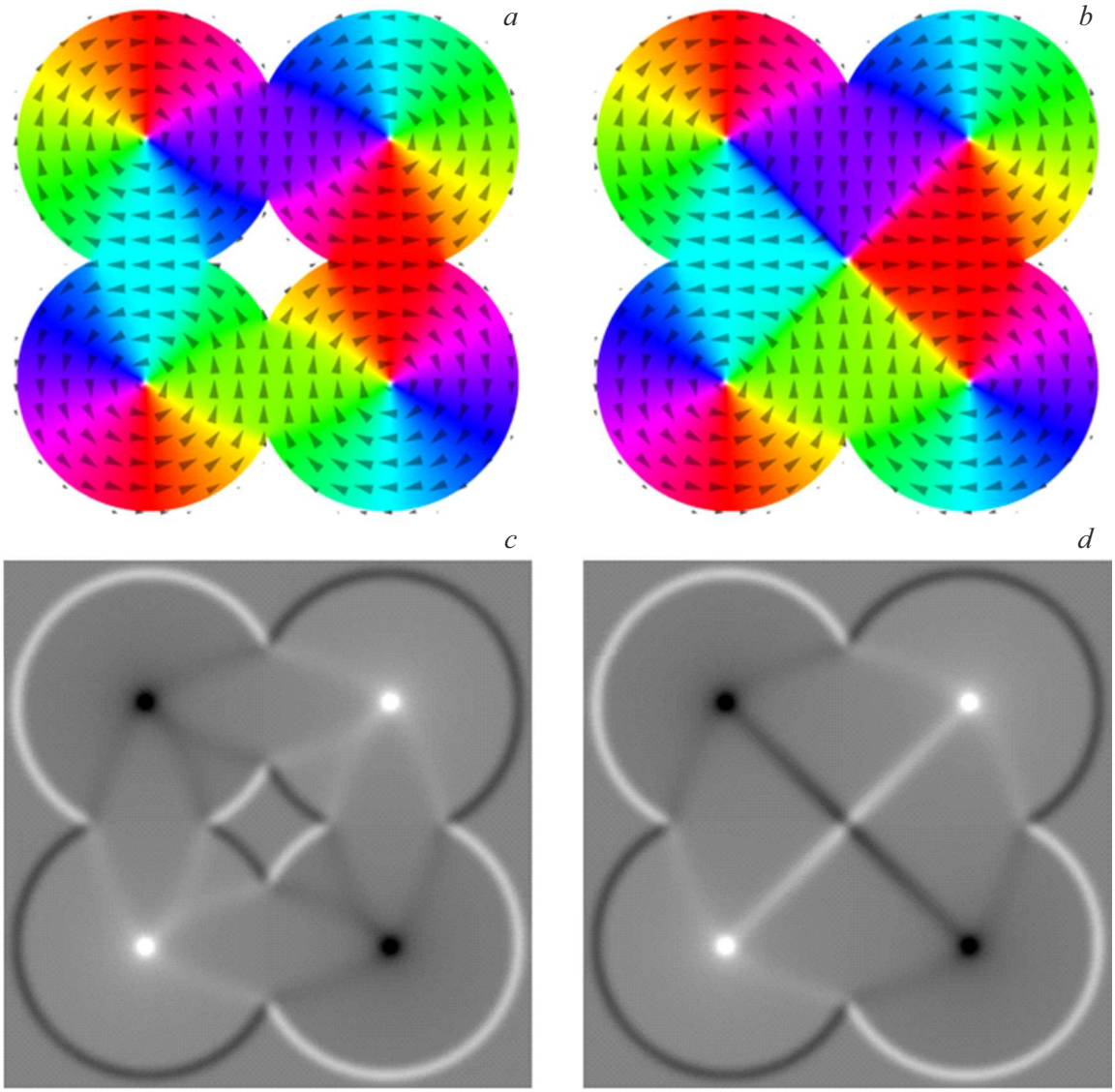

Figure 1. *a, b* — simulated magnetization patterns in the particle with and without hole with alternating vortex shell vorticities; *c, d* — design Fresnel contrast for corresponding magnetization patterns.

In the second case, when shell vorticities of the neighboring vortices coincide in pairs, antivortices are formed between vortices with the same shell vorticity for both types of particles. Whereas in the particle without hole in the center, a quasi-uniform magnetized domain is formed and is oriented approximately on the diagonal of the particle (Figure 2).

Typical microdiffraction rings are shown in Figure 3. It can be seen that the microdiffraction patterns differ considerably. Thus, for mesoparticles produced by the first lithography method, the microdiffraction images have additional weak rings compared with a set of diffraction rings on a mesoparticle produced by the second lithography method without additional metallic masks. The analysis has shown that the main set of rings corresponds to the Py film that has a structural type of Cu with face-centered cubic lattice and space group $Fm\bar{3}m$ with lattice parameter $a_{\mathrm{Py}} = 0.355\,\mathrm{nm}$. Review additional rings in Figure 3, *a* according to materials used in the auxiliary metallic masks. Thus, Cu has the table lattice parameter $a_{\mathrm{Cu}} = 0.360\,\mathrm{nm}$, and its structural type coincides with the Py film structure. Therefore, when a microdiffraction pattern has any rings associated with the Cu film, they cannot be identified against the background of more intensive rings from the Py film. Pt also crystallizes in the structural type of Cu with lattice parameter $a_{\mathrm{Pt}} = 0.392\,\mathrm{nm}$, which differs considerably from Cu and from Py. However, there are no rings corresponding to the Pt film on the microdiffraction. The last element that was used as a protective metallic layer was vanadium (V). It crystallizes in the structural type of tungsten (W) with body-centered lattice and space symmetry group $Im\bar{3}m$ with lattice parameter $a_V = 0.303\,\mathrm{nm}$. Actually, additional

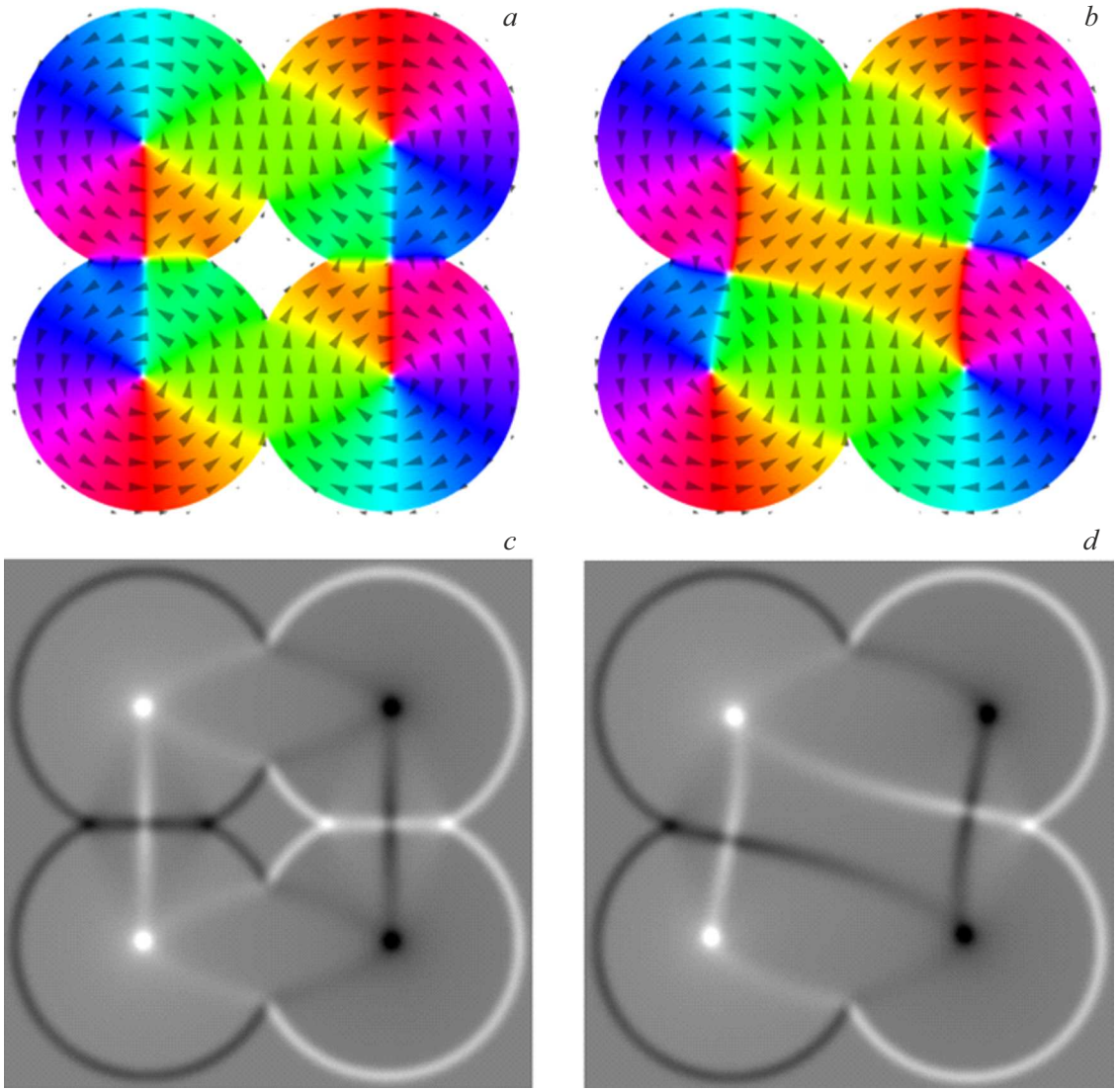

Figure 2. *a, b* — simulated magnetization patterns in the particle with and without hole with pair-coincident vortex shell vorticities; *c, d* — design Fresnel contrast for corresponding magnetization patterns.

microdiffraction rings that are present in Figure 3, *a*, but are absent in Figure 3, *b*, may be unambiguously associated with the V film.

The method of analytical transmission electron microscopy was used to make bright-field micrographs of the patterned mesoparticle fragments (Figure 4, *a, b*). Bright regions on the micrograph correspond to the silicon nitride membrane, while the mesoparticle themselves have a fine polycrystalline structure. Autocorrelation analysis of micrographs has shown that nanocrystallite size for a sample produced by the first lithography method is equal to 11 ± 2 nm, and in the second case nanocrystallite size is equal to 10 ± 2 nm. The difference of the mean sizes is not significant and it is suggested that the films have similar nanostructural properties.

Quality of the particle edge can be estimated by analyzing the azimuth-averaged profile of the bright-field contrast along the radial direction from the disc center (blue and red lines in Figure 4, *a, b*). The mean normalized contrast is shown in Figure 4, *c*, level „0.0“ corresponds to the particle, and „1.0“ corresponds to the membrane of silicon nitride. A mark at which the contrast intersects level „0.5“ may be assumed as the particle edge. It is shown that, when using the first lithography method with additional metallic masks and multistage ionic and plasma-enhanced chemical etching processes, the particle edge is not so sharp and some amount of magnetic material remains outside the formal particle boundary (at a distance of 50–100 nm in Figure 4, *c*). In addition, such smooth boundary has its lateral dimensions several times as large as the mean nanocrystallite size and cannot be associated with individual crystallites outside the particle boundary. Moreover, it is obvious that the proximity effects for the first lithography method have significant negative effect

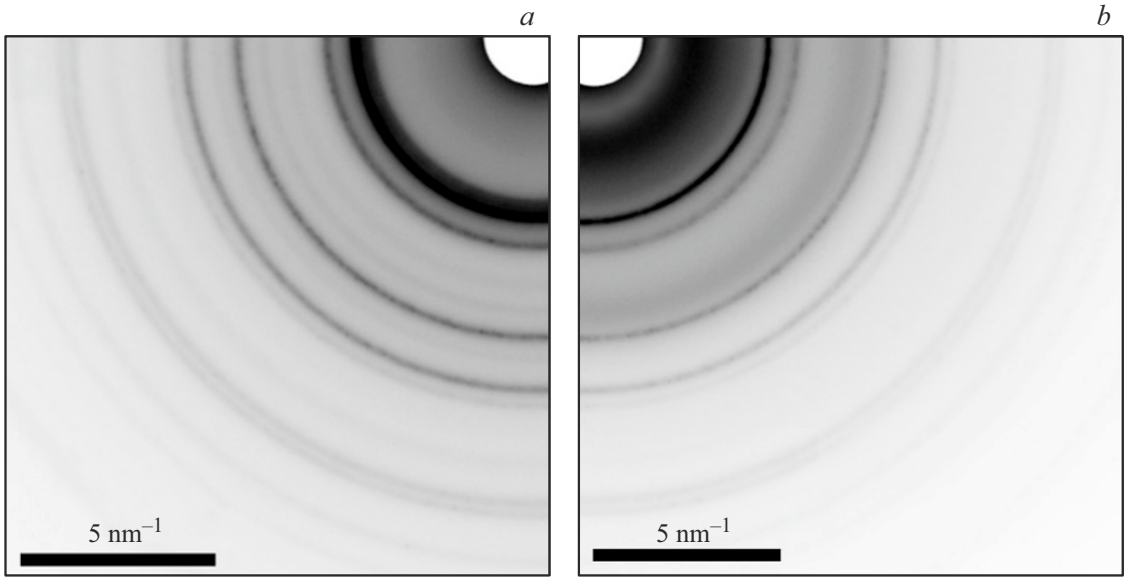

Figure 3. Fragment of electron microdiffraction patterns for mesoparticles produced by the first (a) and second (b) lithography methods.

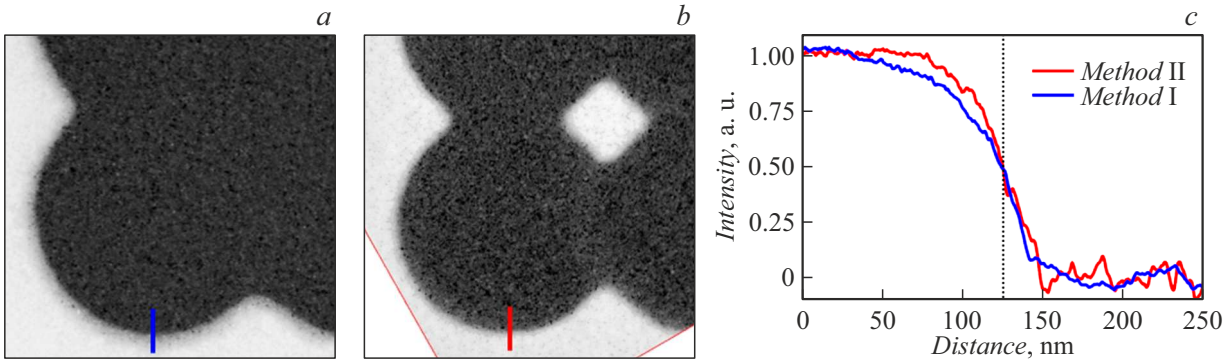

Figure 4. a, b — bright-field microphotographs of the patterned mesoparticle fragment with and without the central hole; c — averaged bright-field contrast with respect to azimuth in radial direction (blue and red lines on (a) and (b)).

during electron-beam resist exposure, which prevents from achievement of a rhombic hole in the center of the particle (Figure 4, a).

When using the second lithography method without additional metallic masks followed by low-voltage ionic argon etching, it is possible not only to produce a particle with a sharper edge, but also to etch a hole with a regular rhombic shape between the discs (Figure 4, b).

The Fresnel test data for the produced particles are shown in Figure 5. By comparing Figure 5, $a-c$ with the corresponding simulations (Figure 1, c, d; 2, d), it can be seen that states obtained by the micromagnetic simulation method are actually formed in particles, except one case. domain walls, rather than antivortices, are formed in the particle with the hole in the center in case of pair-coincident vorticities of neighboring vortices (Figure 2, c), and the vortex centers themselves are shifted towards the particle edges (Figure 5, d).

Conclusions

The proposed second electron-beam lithography system with low-voltage ionic argon etching and without using additional metallic masks makes it possible to make good shaped holes in particles and solid films. It is shown that the lithography method without additional metallic masks also considerably improves the sharpness of mesoparticle boundary. Analytical electron-beam microscopy has demonstrated that in both cases the films had a similar nanocrystalline structure. But, on the other hand, despite the multistage etching process in the first lithography method, the particles from Py films still have additional metallic mask (V) residues.

The shape accuracy has also made it possible to form non-simply connected ferromagnetic particles with mutivortex magnetization pattern without singularities such as domain walls or antivortices, which has been also

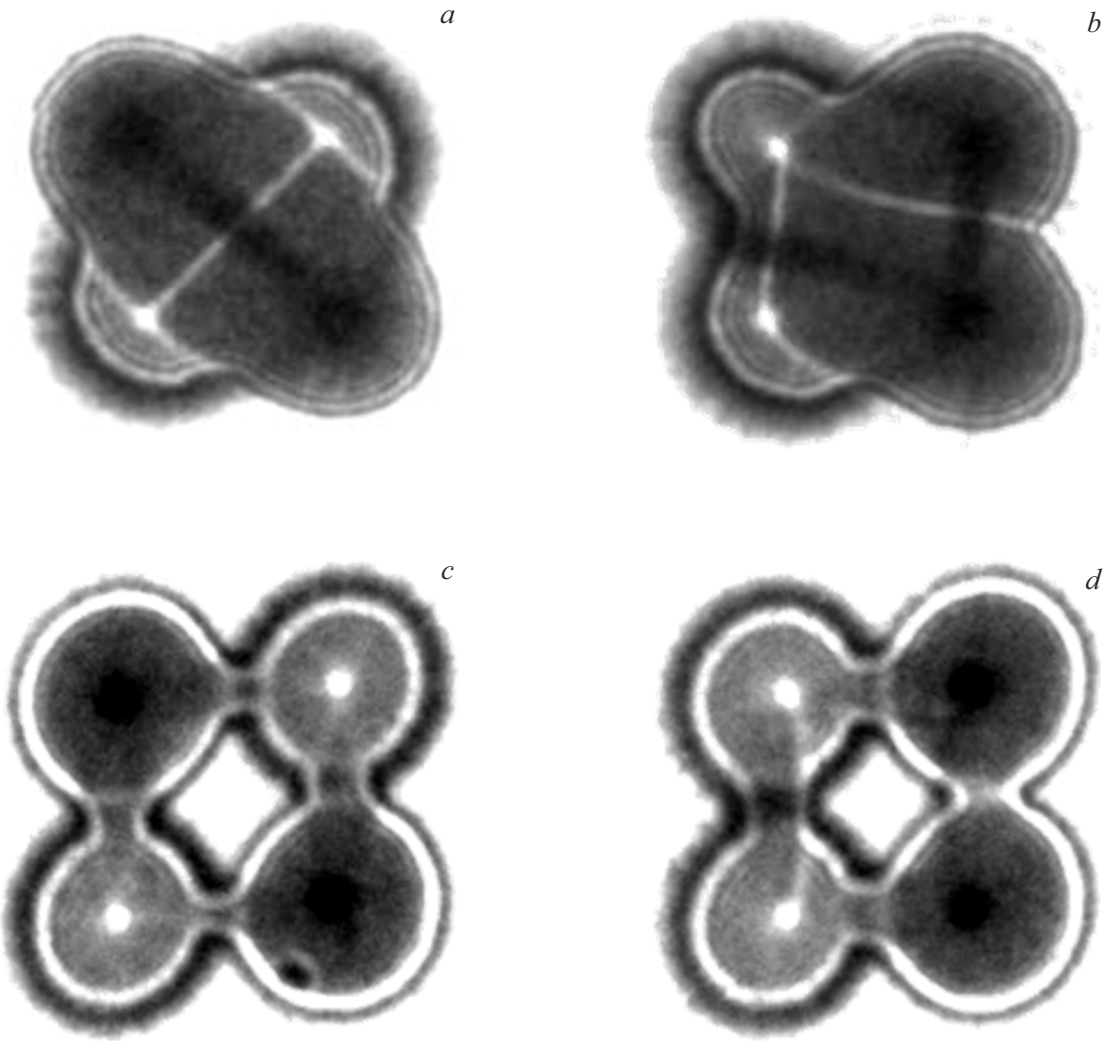

Figure 5. Fresnel contrast in mesoparticles. Vortices with alternating shell vorticity in a solid particle (*a*) and in a particle with hole (*c*); vortices with pair-coincident vorticity in a solid particle (*b*) and in a particle with hole (*d*).

demonstrated by the Fresnel method using the Lorentz transmission electron microscopy.

Funding

Th study was supported by grant of the Russian Science Foundation № 21-72-10176. The study used the equipment provided by the Common Use Center „Physics and Technology of Micro- and Nanostructures“ (Institute for Physics of Microstructures of the Russian Academy of Sciences).

References

[1] R.P. Cowburn, D.K. Koltsov, A.O. Adeyeye, M.E. Welland, D.M. Tricker. Phys. Rev. Lett., **83**, 1042 (1999). DOI: 10.1103/PhysRevLett.83.1042
[2] K.L. Metlov, Y. Lee. Appl. Phys. Lett., **92**, 11 (2008). DOI: 10.1063/1.2898888
[3] D.A. Tatarsky, V.L. Mironov, A.A. Fraerman. ZhETF **142**, 366 (2023) (in Russian). DOI: 10.31857/S0044451023030082
[4] K.S. Buchanan, P.E. Roy, M. Grimsditch, F.Y. Fradin, K.Yu. Guslienko, S.D. Bader, V. Novosad. Nat. Phys., **1**, 172 (2005). DOI: 10.1038/nphys173
[5] L.S. Metlov. Pis'ma v ZhETF **118**, 95 (2023). (in Russian). DOI: 10.31857/S1234567823140057
[6] D.A. Tatarskiy, A.N. Orlova, E.V. Skorokhodov, I.Yu. Pashenkin, V.L. Mironov, S.A. Gusev. JMMM, **590**, 171580 (2024). DOI: 10.1016/j.jmmm.2023.171580
[7] M. Schneider, H. Hoffmann, J. Zweck. Appl. Phys. Lett., **77**, 2909 (2000). DOI: 10.1063/1.1320465
[8] S.A. Nepijko, G. Schönhense. Appl. Phys. A, **96**, 671 (2009). DOI: 10.1007/s00339-009-5131-4
[9] M. Schneider, H. Hoffmann, J. Zweck. Appl. Phys. Lett., **79**, 3113 (2001). DOI: 10.1063/1.1410873
[10] P. Vavassori, N. Zaluzec, V. Metlushko, V. Novosad, B. Ilic, M. Grimsditch. Phys. Rev. B, **69**, 214404 (2004). DOI: 10.1103/PhysRevB.69.214404
[11] S.A. Gusev, D.A. Tatarsky, A.Yu. Klimov, V.V. Rogov, E.V. Skorokhodov, M.V. Sapozhnikov, B.A. Gribkov, I.M. Nefedov, A.A. Fraerman. FTT **55**, 435 (2013) (in Russian).

[12] S.N. Vdovichev, B.A. gribkov, S.A. Gusev, V.L. Mironov, D.S. Nikitushkin, A.A. Fraerman, V.B. Shvetsov. FTT **48**, 1791 (2006) (in Russian).
[13] S. Ma, C. Con, M. Yavuz, Bo Cui. Nanoscale Res. Lett., **6** (1), 446 (2011). DOI: 10.1186/1556-276X-6-446
[14] B. Bilenberg, M. Schøler, P. Shi, M.S. Schmidt, P. Bøggild, M. Fink, C. Schuster, F. Reuther, C. Gruetzner, A. Kristensen. J. Vac. Sci. Technol. B, **24**, 1776 (2006). DOI: 10.1116/1.2210002
[15] S.M. Lewis, G.A. DeRose, H.R. Alty, M.S. Hunt, N. Lee, J.A. Mann, R. Grindell, A. Wertheim, L. De Rose, A. Fernandez, C.A. Muryn, G.F.S. Whitehead, G.A. Timco, A. Scherer, R.E.P. Winpenny. Adv. Func. Mater., **32**, 2202710 (2022). DOI: 10.1002/adfm.202202710
[16] R. Andok, K. Vutova, A. Bencurova, I. Kostic, E. Koleva. J. Phys.: Conf. Ser., **2443**, 012006 (2023). DOI: 10.1088/1742-6596/2443/1/012006
[17] K. Kato, Y. Liu, Sh. Murakami, Y. Morita, T. Mori, Nanotech., **32**, 485301 (2021). DOI: 10.1088/1361-6528/ac201b
[18] I. Zailer, J.E.F. Frost, V. Chabasseur-Molyneux, C.J.B. Fordand, M. Pepper. Semicond. Sci. Technol., **11**, 1235 (1996). DOI: 10.1088/0268-1242/11/8/021
[19] H. Yang, A. Jin, Q. Luo, J. Li, Ch. Gu, Z. Cui. Microelectron. Engineer., **85**, 814 (2008). DOI: 10.1016/j.mee.2008.01.006
[20] P. Schnauber, R. Schmidt, A. Kaganskiy, T. Heuser, M. Gschrey, S. Rodt, S. Reitzenstein. Nanotech., **27**, 195301 (2016). DOI: 10.1088/0957-4484/27/19/195301
[21] D.A. Tatarskiy, N.S. Gusev, S.A. Gusev. Ultramicroscopy, **253**, 113822 (2023). https://doi.org/10.1016/j.ultramic.2023.113822
[22] D.G. Reunov, N.S. Gusev, M.S. Mikhailenko, D.V. Petrova, I.V. Malyshev, N.I. Chkhalo. ZhTF, **93** (7), 1032 (2023). (in Russian). DOI: 10.21883/JTF.2023.07.55765.105-23
[23] R. Heilbronner. Tectonophysics, **212**, 351 (1992). DOI: 10.1016/0040-1951(92)90300-U
[24] B. Zang, K. Suzuki, A. Liu. Mater. Characterization, **142**, 577 (2018).
[25] A. Vansteenkiste, J. Leliaert, M. Dvornik, M. Helsen, F. Garcia-Sanchez, B. Van Waeyenberg. AIP Adv., **4**, 107133 (2014). DOI: 10.1063/1.4899186
[26] S. McVitie, M. Cushley. Ultramicroscopy, **106**, 423 (2006). DOI: 10.1016/j.ultramic.2005.12.001

Translated by E.Ilinskaya